HHS Public Access

Author manuscript

Sci Signal. Author manuscript; available in PMC 2019 June 11.

Published in final edited form as:

Sci Signal. ; 11(560): . doi:10.1126/scisignal.aau0144.

Restricting mitochondrial GRK2 post-ischemia confers cardioprotection by reducing myocyte death and maintaining glucose oxidation

Priscila Y. Sato[1,2,3], **J. Kurt Chuprun**[1,2], **Laurel A. Grisanti**[1,2,4], **Meryl C. Woodall**[1,2], **Brett R. Brown**[1,2], **Rajika Roy**[1,2], **Christopher J. Traynham**[1,2], **Jessica Ibetti**[1,2], **Anna M. Lucchese**[1,2], **Ancai Yuan**[1,2], **Konstantinos Drosatos**[1,2], **Doug G. Tilley**[1,2], **Erhe Gao**[1,2], and **Walter J. Koch**[1,2,*]

[1]Center for Translational Medicine, Lewis Katz School of Medicine, Temple University, Philadelphia, PA 19140, USA.

[2]Department of Pharmacology, Lewis Katz School of Medicine, Temple University, Philadelphia, PA 19140, USA.

[3]Department of Pharmacology and Physiology, Drexel University College of Medicine, Philadelphia, PA, 19102, USA.

[4]Department of Biomedical Sciences, College of Veterinary Medicine, University of Missouri, Columbia, MO 65211, USA.

Abstract

Increased abundance of GRK2 [G protein–coupled receptor (GPCR) kinase 2] is associated with poor cardiac function in heart failure patients. In animal models, GRK2 contributes to the pathogenesis of heart failure after ischemia-reperfusion (IR) injury. In addition to its role in down-regulating activated GPCRs, GRK2 also localizes to mitochondria both basally and post-IR injury, where it regulates cellular metabolism. We previously showed that phosphorylation of GRK2 at Ser^{670} is essential for the translocation of GRK2 to the mitochondria of cardiomyocytes post-IR injury in vitro and that this localization promotes cell death. Here, we showed that mice with a S670A knock-in mutation in endogenous GRK2 showed reduced cardiomyocyte death and better cardiac function post-IR injury. Cultured GRK2-S670A knock-in cardiomyocytes subjected to IR in vitro showed enhanced glucose-mediated mitochondrial respiratory function that was partially due to maintenance of pyruvate dehydrogenase activity and improved glucose oxidation. Thus, we

*Corresponding author. walter.koch@temple.edu.

Author contributions: P.Y.S. conducted experiments and wrote the paper. E.G. and R.R. did IR surgeries. A.Y. and A.M.L. did the hemodynamic experiments. A.M.L. performed Western blots. P.Y.S., B.R.B., and K.D. performed glucose oxidation experiments. M.C.W. performed migration studies. L.A.G. and D.G.T. performed βAR density studies. J.I. and C.J.T. provided technical support and scientific input to the work. J.K.C. and W.J.K. generated the hypothesis for the work, contributed to data analysis and interpretation, and wrote the paper.

Competing interests: The authors declare that they have no competing interests.

Data and materials availability: All data needed to evaluate the conclusions in the paper are present in the paper or the Supplementary Materials. A material transfer agreement is required by Temple University for the GRK2-S670A KI mice.

propose that mitochondrial GRK2 plays a detrimental role in cardiac glucose oxidation post-injury.

INTRODUCTION

Genes encoding seven-transmembrane–spanning, G protein–coupled receptors (GPCRs) comprise one of the largest families in the human genome. In the heart, a class of GPCRs known as β-adrenergic receptors (βARs) promotes cardiac contractility. Upon activation of βARs, GPCR kinases (GRKs) phosphorylate the receptor, leading to the recruitment of β-arrestin and subsequent clathrin-mediated receptor recycling or down-regulation (1). In heart failure (HF) patients and in animal models, levels of GRK2 inversely correlate with cardiac function and HF development post-injury. Cardiac expression of a peptide inhibitor of GRK2 (2, 3) or deletion of GRK2 pre- or post- injury (4) is cardioprotective and even reverses cardiac dysfunction in HF. Conversely, cardiac overexpression of GRK2 results in a detrimental cardiac outcome post-injury (3). Although the role of GRK2 in mediating canonical GPCR signaling in the cytoplasm has been extensively elucidated, GRK2 also localizes to mitochondria (5–7) where it plays a metabolic role.

Augmented cardiac GRK2 levels have been reported in diabetic mouse models and mice after a high-fat diet (8). Moreover, GRK2 heterozygous knockout mice are resistant to weight gain when fed a high-fat diet (9), whereas GRK2 deletion in mice leads to more weight gain on a high-fat diet (10). In a mouse model of fatty acid synthase overexpression, coexpression of a GRK2 inhibitor peptide improves mitochondrial metabolism and delays the development of HF (11). Furthermore, by restoring glucose homeostasis, suppression of GRK2 has been linked to improved endothelial function (12). Overall, functional and biochemical evidence support a negative metabolic role for GRK2.

The kinase activity of GRK2 relies on Lys^{220} (13). Phosphorylation of Ser^{670} in GRK2 by mitogen-activated protein kinases (MAPKs) such as ERK is critical in promoting GPCR phosphorylation (14). Although kinase activity depends on Lys^{220}, phosphorylation of GRK2 at Ser^{670} substantially decreases the ability of GRK2 to phosphorylate GPCRs (13, 14). We have shown that the ERK-mediated phosphorylation of GRK2 at Ser^{670} is involved in the translocation of GRK2 to mitochondria after cellular oxidative stress and this localization detrimentally affects mitochondrial function and promotes cell death (5, 15). Moreover, in renal radiofrequency ablation, cardiac protection post-IR (ischemia-reperfusion) injury has been linked to diminished phosphorylation of Ser^{670} in GRK2 (16). RGS6 knockout mice show increased infarct size post-IR injury that has been attributed to augmented phosphorylation of GRK2 localized to mitochondria (17). Although substantial evidence supports the notion that increased GRK2 abundance inhibits cardiac function and metabolism, the specific role of mitochondrial GRK2 in affecting cardiac outcome after injury in vivo, including cardiac metabolism, remains unknown. To further investigate the role of Ser^{670} of GRK2 in the heart, we generated a GRK2 knock-in (KI) mouse that harbors a serine to alanine point mutation at residue 670 (GRK2-S670A) and characterized these mice after IR injury.

RESULTS

GRK2-S670A KI mice show normal cardiac function and morphology at baseline

In addition to sequencing for the correct genomic mutation (fig. S1, A and B), we confirmed the lack of phosphorylation at Ser^{670} in GRK2 immunoprecipitated from heart lysates of wild-type (WT) and GRK2- S670A KI mice using a site-specific antibody that recognizes phosphorylation at this site. There was no signal for phosphorylated Ser^{670} in the GRK2-S670A KI animals when compared to WT animals (Fig. 1A). In addition, total GRK2 levels were similar between GRK2-S670A KI and WT hearts (Fig. 1, B and C) and brains (fig. S1C). Heart weight–to–body weight (Fig. 1D) or heart weight–to–tibia length (fig. S1D) ratios indicated no major gross anatomical change in the GRK2-S670A KI mice. Cardiac function as measured by echocardiography and hemodynamics were similar between WT and GRK2-S670A KI animals (Fig. 1, E and F, and fig. S1E). In addition, the GRK2-S670A mutation did not affect total cardiac βAR levels, as assessed by radioactive-ligand binding assays performed on isolated plasma membranes from WT and GRK2-S670A KI hearts (Fig. 1G). Transmission electron microscopy showed normal ultrastructural morphology in the hearts of GRK2-S670A KI mice (Fig. 1H). In addition, based on a previous report showing a potential role for Ser^{670} in cell migration (18), we performed migration experiments on WT and GRK2-S670A KI adult cardiac fibroblasts, which showed similar migratory characteristics (fig. S2).

IR injury leads to GRK2 mitochondrial translocation in vivo that depends on Ser^{670}

We conducted myocardial IR injury (30-min ischemia followed by 24 hours of reperfusion) as previously described (19) to determine effects on subcellular localization of GRK2 in vivo. IR injury did not change total levels of GRK2 at the myocardial area at risk (AAR), as determined by Western blot analysis (Fig. 1I and fig. S3A). However, Western blot analysis of purified mitochondrial fractions prepared from the AAR revealed significant accumulation of WT GRK2 post-IR injury compared to the sham group, and this change in GRK2 localization was absent in lysates from GRK2-S670A KI mice (Fig. 1, J and K). These findings indicate that the phospho rylation of Ser^{670} in GRK2 is required for mitochondrial translocation post-IR injury in vivo and that an absence of phosphorylation at this residue retains this kinase in the cytoplasm after ischemic injury. In support of the Western blot experiments, immunogold labeling of GRK2 at the AAR showed that post-IR injury localization of GRK2 to mitochondria in GRK2-S670A KI mice was significantly decreased when compared to WT mice (Fig. 1L and fig. S3B).

Limiting GRK2 mitochondrial accumulation restricts infarct size and cell death post-IR injury and improves cardiac function

Infarct size as measured by Evans blue/ tetraphenyl tetrazolium chloride (TTC) staining revealed that GRK2-S670A KI mice had smaller infarcts than WT mice, suggesting that eliminating phosphorylation at Ser^{670} and post-IR injury mitochondrial localization ameliorates injury (Fig. 2, A to C). Upon injury, the heart releases troponin I in the bloodstream (16). GRK2-S670A KI mice had significantly less troponin I when compared to WT animals post-IR injury, consistent with the infarct data (Fig. 2D). The apoptotic index of cardiomyocytes as assessed by TUNEL (terminal deoxynucleotidyl transferase–mediated

deoxyuridine triphosphate nick end labeling) staining demonstrated that GRK2-S670A KI hearts had significantly fewer apoptotic myocytes compared to WT hearts post-IR injury (Fig. 2, E and F). The decreased cell death in GRK2-S670A KI mice post- IR injury was physiologically important because these mice had significantly improved cardiac function compared to WT mice post-IR injury, similar to that in sham- operated WT mice (Fig. 2, G and H).

Mitochondrial oxygen consumption rates are improved in GRK2-S670A KI adult cardiomyocytes post-IR injury

To assess the role of mitochondrially accumulated GRK2 after ischemic injury, we assessed mitochondrial oxygen consumption rates (OCRs) in adult ventricular cardiomyocytes isolated and exposed to IR. First, we established that the ischemic protocol elicited cellular changes (fig. S4). As expected, WT cardiomyocytes had a decrease in basal respiration and adenosine 5′-triphosphate (ATP)–linked respiration post-IR injury, whereas cardiomyocytes from GRK2-S670A KI mice showed significantly improved basal respiration and ATP-linked respiration (Fig. 3, A to C, and fig. S4). These results suggest that GRK2-S670A KI cardiomyocytes recover more quickly from ischemic insults compared to WT cells. In addition, the maximal respiration rate was comparable among all groups, suggesting that the proton gradient was most likely being consumed by uncoupling proteins (20). Although adult cardiomyocytes can use fatty acids and glucose as substrates for ATP production, substrate preference can vary depending on the cardiac pathology (21). To determine the role of each substrate in eliciting respiration post-IR injury, we used 2-deoxyglucose (2-DG) to inhibit glucose-mediated respiration and etomoxir to inhibit fatty acid oxidation. As expected, WT cardiomyocytes had a significant decrease in glucose-mediated respiration post-IR injury, which was not evident in myocytes isolated from GRK2-S670A KI mice (Fig. 3, D to F).

Mitochondrial accumulation of myocardial GRK2 post-IR injury decreases pyruvate dehydrogenase activity and glucose utilization

To assess the role of Ser^{670} and mitochondrial localization post-IR injury in glucose oxidation, we assessed various checkpoints at which glucose metabolism could be affected. βAR signaling has been linked to modulating glucose metabolism (22); however, plasma membrane βAR density did not differ between WT and GRK2-S670A KI groups (Fig. 4A). Cardiomyocytes express both the insulin-sensitive glucose transporter 4 (GLUT4) and the insulin-insensitive GLUT1. Western blotting analysis showed that neither of these proteins were altered in abundance in plasma membranes isolated from WT or GRK2-S670A KI hearts (Fig. 4, B to E). The rate-limiting enzyme for aerobic glucose oxidation is pyruvate dehydrogenase (PDH), and the activity of this enzyme is thought to decrease after ischemic injury (23–25). Myocardial lysates from the AAR of post-IR injury WT mice had decreased PDH activity, although PDH activity was not decreased in GRK2- S670A KI hearts compared to sham hearts (Fig. 4F) and showed improved glucose oxidation rates (Fig. 4G).

DISCUSSION

We have previously shown that myocardial GRK2 mitochondrial translocation and accumulation post-ischemic and oxidative stress is mediated by ERK- mediated phosphorylation of GRK2 at Ser^{670} (5). Phosphorylation at this site decreases the ability of GRK2 to phosphorylate membrane-bound GPCRs (14). In addition, cardioprotection post-IR injury in animals subjected to renal radiofrequency ablation has been attributed to decreased phosphorylation of GRK2 at residue Ser^{670} (16). To investigate the role of Ser^{670} phosphorylation in vivo, we generated KI mice expressing a form of GRK2 that could not be phosphorylated at Ser^{670} (GRK2-S670A KI). This mutation, which was present in mice from conception, did not produce any obvious phenotype, and all measured cardiac parameters were normal. We also found that basal levels of GRK2 in the heart (and other organs) were comparable in GRK2-S670A KI mice and WT control mice. This is relevant because Ser^{670} phosphorylation potentially affected total protein levels of GRK2, although proteasomal degradation is primarily carried out by c-src–mediated phosphorylation of Tyr^{13}, Tyr^{86}, and Tyr^{92} (26).

GRK2-S670A KI mice did not show any basal differences. However, when we stressed the mice with IR, GRK2 levels were substantially increased in myocardial mitochondria from the AAR of post-IR injury WT mice. Thus, it appears that phosphorylation of Ser^{670} promotes pathological GRK2 mitochondrial translocation after stress. This increase in mitochondrial GRK2 in WT mice was not due to increased de novo expression of this kinase after injury. In addition, the baseline levels of GRK2 seen within mitochondria did not depend on Ser^{670} or its phosphorylation status. One explanation is that there are two pools of mitochondrial GRK2: (i) the basal pool of unphosphorylated GRK2 and (ii) post-stress, phosphorylated GRK2 at Ser^{670}. This site is missing in the homolog of GRK2 in lower species, *Gprk2* (27), potentially suggesting a mode of regulation that has evolved in higher species. Thus, GRK2 that is basally localized to mitochondria could have a role that is different than the phosphorylated GRK2 that accumulates at mitochondria in response to stress. Unphosphorylated GRK2 could play a role in membrane GPCR signaling in the mitochondria, whereas the phosphorylated GRK2 mediates activity with non-GPCR substrates because the phosphorylation of Ser^{670} decreases the ability of GRK2 to phosphorylate GPCRs (15). Future studies will be required to delineate these non-canonical targets of mitochondrial GRK2.

We observed that the GRK2-S670A KI mice had smaller infarcts than WT mice because of substantially decreased myocyte death post-IR injury. The substantial increase in viable myocardium, which was corroborated by lower troponin levels in the serum of post-IR injury GRK2-S670A KI mice, resulted in prevention of in vivo cardiac dysfunction 24 hours post- ischemic injury, as assessed by echocardiography. These results support our hypothesis that translocated GRK2 after Ser^{670} phosphorylation is associated with prodeath activity of GRK2.

Although the heart is an organ with high energy consumption, it depends on mitochondria for ATP production almost entirely on a beat-to-beat basis. It is at the mitochondrial level that metabolic substrates ultimately fuel the electron transport chain to generate ATP, which

subsequently promotes contraction and cell viability. The heart mainly uses fatty acids and glucose as energy sources, although substrate preference is altered in various cardiac pathologies and implicated in disease development (21, 24). Ischemic injury may lead to altered cardiac metabolism, mainly due to a mismatch between oxygen availability and demand. During ischemia, glycolysis speeds up, whereas glucose oxidation decreases (24). The PDH complex converts pyruvate to acetyl–coenzyme A (CoA) and is the rate-limiting step linking glycolysis to glucose oxidation. Stimulation of PDH activity post-injury enhances cardiac recovery (28, 29), and in a genetic mouse model that causes the accumulation of branched-chain amino acids, decreased PDH activity correlates with poor cardiac function post-IR injury, an effect that is partially rescued by overexpressing GLUT1 to enhance glucose metabolism (30).

As an additional supporting mechanism for cardioprotection after ischemic injury in GRK2-S670A KI mice, we found substantially improved basal mitochondrial respiration and maintenance of ATPlinked respiration in isolated adult ventricular myocytes post-IR injury. Thus, phosphorylated GRK2 localized to mitochondria after ischemic injury not only promotes cell death but also depresses mitochondria function. Glucose utilization contributes to the metabolic response post-IR injury because cardiac glucose oxidation substantially decreases after ischemic injury, although glycolysis is maintained (24, 31, 32). Instead of the depression in glucose-mediated respiration observed in post-IR injury WT myocytes, GRK2-S670A KI myocytes showed improved glucose-mediated oxidation post-IR injury. Administration of the pyruvate analog ethyl pyruvate to rats before IR injury is cardioprotective and attenuates oxidative injury because it maintains mitochondrial function (29). Thus, GRK2 may be a nodal regulator of the prodeath and metabolic functions of mitochondria.

Glucose utilization can be influenced at several steps in cardiomyocytes; however, the post-IR injury abundance of βAR and GLUT1/4 was similar between WT and GRK2-S670A KI mice. Thus, the loss of Ser^{670} regulation does not appear to influence GRK2 activity toward βARs in our experimental time frame. Last, PDH is a mitochondrial enzyme, involved in the rate-limiting step of glucose oxidation converting pyruvate to acetyl-CoA (24). As expected, upon injury, WT cardiac tissue from the AAR showed a statistically significant decrease in PDH activity, as previously shown (25, 33). However, GRK2-S670A KI mice showed improved PDH activity post-IR injury. This result suggests that the decrease in PDH post-IR injury is mediated by GRK2 that accumulates in mitochondria after ischemic stress. Mechanistically, this can explain the maintenance of glucose-mediated respiration and ATP-linked respiration after ischemic injury in the GRK2-S670A KI mice. Future studies will be required to determine whether PDH is a direct substrate of GRK2 or whether this regulation is indirect.

The current findings are consistent with and extend our previous report that in isolated cardiomyocytes, mitochondrial GRK2 levels increase in response to oxidative stress. Our studies agree with previous reports describing a detrimental role for mitochondrial GRK2 (11, 12, 16, 17). Our in vivo study supports the idea of an important noncanonical role for GRK2 in mitochondria, broadening the perspective for novel therapeutic approaches in treating and preventing acute coronary syndromes. Further studies detailing the precise

mechanism of the impact of mitochondrial GRK2 on cardiac metabolism still remain to be determined. Overall, coupled with its effects on adrenergic inotropic reserve, GRK2 appears to be a nodal point of regulation between myocyte metabolism and contractility.

MATERIALS AND METHODS

Generation of GRK2-S670A KI mice

A Ser^{670}→Ala^{670} (S670A) mutation was generated in the *Adrbk1* gene located in exon 21. A ~9.86-kb region used to construct the targeting vector was first subcloned from a positively identified C57BL/6 bacterial artificial chromosome (BAC) clone (RP23: 28A2). The region was designed such that the long homology arm extends ~5.88 kb 3′ to the site of the point mutations (T→G) in exon 21 and the FRT-flanked Neo cassette is inserted 1.74 base pair (bp) 5′ to the point mutations. The short homology arm extends 2.24 kb 5′ to the FRT-flanked Neo cassette. The targeting vector was constructed using Red/ET recombineering technology. The BAC was subcloned into a ~2.4-kb backbone vector (pSP72, Promega) containing an ampicillin selection cassette for retransformation of the construct before electroporation. A pGK-gb2 FRT Neo cassette was inserted into the gene. The targeting construct was linearized using Not I before electroporation into embryonic stem cells. Positive clones were injected to generate chimeric mice and GRK2-S670A mice (inGenious Targeting Laboratory). Mutation was confirmed by polymerase chain reaction products flanking exon 21. Screening was performed using the primers 5′-GGGTGTGTCACAGTTGGAACC-3′ and 5′-GGGCTCTGCACCATTCAAGTTGAG-3′.

IR injury model

Surgical procedures were carried out according to the National Institutes of Health (NIH) *Guide for the Care and Use of Laboratory Animals*, and all procedures were approved by the Institutional Animal Care and Use Committee at Temple University Lewis Katz School of Medicine. The IR injury protocol was performed as previously described (34). Briefly, 13- to 15-week-old male mice were anesthetized with 3% isoflurane. The heart was exposed through a left thoracotomy at the level of the fourth intercostal space. A slipknot was inserted around the left anterior descending coronary artery (LAD) at the level of the left auricle with a 6–0 silk suture. After the ligature of the slipknot, the heart was immediately placed back into the intrathoracic space followed by evacuation of pneumothoraces and closure of the muscle and skin. Sham-operated animals were subjected to the same operation, except the suture was passed under the LAD but not tied. After 30 min of ischemia, the slipknot was released, and the myocardium was reperfused for 24 hours unless otherwise denoted.

Determination of LV infarct size and AAR

LV infarct size and AAR were determined as previously described (34). The ligature around the LAD was retied through the previous ligation, and 0.2 ml of 2% Evans blue dye was injected retrogradely through the aorta after 24 hours of reperfusion. The dye distributed in the heart to areas perfused by the nonligated coronary arteries. The heart was then excised and sliced into five 1.2-mm-thick sections in the short-axis orientation. The sections were then stained with 2% TTC (Sigma-Aldrich) in phosphate-buffered saline (PBS), followed by

PBS-only incubation, and digitally photographed. Infarct area was the TTC-negative staining region. The AAR consisted of the Evans blue–negative region (TTC-positive and TTC-negative regions). The ANAR consisted of Evans blue–positive regions. These regions were quantified by SigmaScan Pro (SPSS Science). Myocardial percentage of AAR was computed as the infarct area/AAR, and the AAR was calculated as a percentage total LV [AAR/(AAR + ANAR)].

Transthoracic echocardiographic analysis

Vevo 2100 transthoracic two-dimensional echocardiography was performed in mice anesthetized with 2% isoflurane, as described previously (34). M-mode echocardiography was carried out in the parasternal short-axis view in mice of baseline animals or mice 24 hours after the IR injury protocol. LV fractional shortening and ejection fraction were calculated offline using Vevo software analysis.

Hemodynamic analysis of cardiac function

Hemodynamic analysis in vivo was performed as previously described (34, 35). Briefly, mice were anesthetized with avertin, and a 1.4-French micromanometer-tipped catheter (Millar Instruments) was inserted into the right carotid artery and then advanced into the LV. A polyethylene-50 catheter was placed in the left external jugular vein for incremental infusion of isoproterenol. Steady-state LV maximal (dP/dt) was recorded in closed-chest mode throughout the experiment with PowerLab DAQ System (Millar Instruments).

Assessment of myocardial apoptosis

Myocardial apoptosis was performed as previously described (34) with minor modifications. Sham- or IR-operated mice were euthanized 4 hours after reperfusion, and hearts were quickly removed and fixed in 4% paraformaldehyde. The hearts were then exposed to sucrose and cryofixed. Hearts were then sectioned on a cryostat with sections measuring 5 μm in thickness. TUNEL staining was carried out with the In Situ Cell Death Detection Kit as per the manufacturer's protocol (Roche). Slides were counterstained with α-actinin (Sigma A7811) and DAPI to label cardiomyocytes and nuclei, respectively. Slides were mounted with Fluoromount-G (Southern Biotech), and images were acquired with a 20× objective on a Nikon TiE fluorescence microscope. The apoptotic index was determined by using NIS- Elements Software (Nikon, Japan). On average, about 7000 cells were counted per heart.

Isolation of adult cardiac myocytes

Adult mice were anesthetized with 3% isoflurane and injected with 200 U of heparin 5 min before heart excision. The heart was quickly cannulated and retrogradely exposed to perfusion buffer (120.4 mM NaCl, 14.7 mM KCl, 0.6 mM KH_2PO_4, 0.6 mM Na_2HPO_4, 1.2 mM $MgSO_4$, 10 mM Hepes, 4.6 mM $NaHCO_3$, 30 mM taurine, 10 mM BDM (2,3-butanedione monoxime), and 5.5 mM glucose) at 37°C. Hearts were then perfused for 12 min with enzyme solution containing 50 mg of collagenase and 0.005% trypsin in perfusion buffer containing 12.5 μM $CaCl_2$. Solution was then switched to perfusion buffer for another 3 min. Atria was removed, and ventricles were gently minced. Cardiomyocytes were

dissociated by pipetting in stop solution (perfusion buffer containing 10% fetal bovine serum and 12.5 μM $CaCl_2$). Cells were serially exposed to increasing amounts of calcium (62 μM to 1 mM).

Isolation of adult fibroblasts and migration assays

Adult cardiac fibroblasts were isolated from 2- to 3-month-old WT and GRK-S670A KI mice, as reported (36, 37). Hearts were excised, rinsed in cold Hank's balanced salt solution, minced, and digested with type II collagenase (100 U/ml) (Worthington) and pancreatin (0.6 mg/ml) (Sigma) at 37°C for 15 min. The first digestion was discarded. The second digestion containing cardiac fibroblasts was centrifuged for 5 min at 3000 rpm and resuspended in Dulbecco's modified Eagle's medium (DMEM) with 10% fetal bovine serum/1% penicillin/streptomycin. The digestion was repeated five to six times, or until the fluid became clear. Cells were plated in 60-mm dishes (Corning, NY) and allowed to attach for 1 hour before the first medium change. During this first medium change, weakly adherent cells (including myocytes and endothelial cells) were removed. Fibroblasts were washed twice with Ca^{2+}- and Mg^{2+}-free PBS (Cellgro, Mediatech Inc.), and plated in 10% DMEM on chamber plates (Ibidi). After 24 hours, the insert was removed and images were acquired at 0, 18, and 24 hours post-removal of the insert with a 10× objective (Nikon TiE microscope).

Isolation of mitochondria from mouse tissue

Mitochondria were prepared from mouse hearts as previously described (5). Briefly, tissue was minced and resuspended in MSH buffer [210 mM mannitol, 70 mM sucrose, 5 mM Hepes (pH 7.5)] supplemented with 1 mM EDTA. Homogenization was performed with a glass/glass dounce homogenizer and centrifuged at 600g for 10 min at 4°C. The supernatant was removed and respun at 600g for 10 min. The resulting supernatant was removed and centrifuged again at 5500g for 20 min at 4°C. The mitochondrial pellet was washed by resuspension in fresh MSH buffer without EDTA and centrifuged again at 5500g for 20 min. The mitochondrial pellet was referred to as the mitochondrial fraction.

Immunoprecipitation and immunoblotting

Tissue or pellets were resuspended in radioimmunoprecipitation assay (RIPA) lysis buffer (150 mM NaCl, 50 mM tris-HCl, 6 mM sodium deoxycholate, 1% NP-40, 1 mM EDTA, 1 mM NaF) supplemented with 1× protease inhibitor (Calbiochem) and 1× phosphatase inhibitor cocktails 2 and 3 (Millipore Sigma). Homogenates were allowed to equilibrate for 1 hour at 4°C, followed by centrifugation (13,000 rpm for 20 min) at 4°C. Supernatant was then collected followed by a protein assay. For immunoprecipitation of GRK2, GRK2 antibody conjugated to agarose was added to 1 mg of total protein and rotated for 1.5 hours at 4°C. Beads were washed three times with RIPA and solubilized in sample buffer. For immunoblotting, samples were prepared in sample buffer and (30 μg) loaded on a 4 to 20% gel and transferred on nitrocellulose membranes. The membrane was blocked in LI-COR block buffer for 1 hour at room temperature, followed by exposure to primary antibody at 4°C. Primary antibodies used were as follows: GRK2 rabbit (Santa Cruz Biotechnology, sc-562), GRK2 mouse (Millipore), rabbit phospho-670 GRK2 (Invitrogen), mouse VDAC (NeuroMab), GLUT1 rabbit (Cell Signaling Technology, 12939), GLUT4 mouse (Cell Signaling Technology, 2213), Gβγ rabbit (Santa Cruz Biotechnology, sc-261), HIF-1α

(Cayman, 10006421), and β-actin mouse (Santa Cruz Biotechnology, 47778). Membranes were washed three times with PBS containing 0.1% Tween-20 and exposed to fluorescent conjugated secondary antibodies: rabbit 680 (Life Technologies, A21109), mouse 680 (Thermo Fisher Scientific, A21058), rabbit 800 (Cell Signaling Technology, 5151S), and/or mouse 800 (Cell Signaling Technology, 5257S). Imaging and quantification were done using LI-COR Odyssey software.

Plasma membrane preparations and radioligand β-receptor measurements

Plasma membrane preparations were purified as described (38). Briefly, membrane preparations from cardiac tissue were prepared by homogenization in ice-cold lysis buffer [25 mM tris (pH 7.4), 5 mM EDTA, aprotinin (1 μg/ml), and leupeptin (1 μg/ml)] and centrifuged at 1000g for 5 min at 4°C. The supernatant was centrifuged at 30,000g, and the crude membrane pellet was resuspended in lysis buffer containing 10% glycerol and stored at −80°C until use. The density of βAR on plasma membranes was determined by saturation binding experiments. Membrane preparations (25 μg of protein) were incubated with [^{125}I]cyanopindolol (200 pM; PerkinElmer) in binding buffer [75 mM tris (pH 7.4), 2 mM EDTA, 12.5 mM $MgCl_2$, aprotinin (1 μg/ml), and leupeptin (1 μg/ml)]. Incubations were performed in the presence or absence of propranolol (10 μM) to determine nonspecific binding. The reactions were performed in a 250-μl volume and allowed to equilibrate at 37°C for 1 hour before filtering the membranes through a glass fiber filter (Whatman GF/C; Brandel). Each filter was washed five times with 5 ml of ice-cold wash buffer [10 mM tris (pH 7.4) and 10 mM EDTA] to remove unbound ligand. The amount of total and nonspecific radiolabel bound to cell membranes was determined on a gamma counter. All assays were performed in triplicate. Receptor density was normalized to milligrams of membrane protein.

Transmission electron microscopy and immunogold-labeled electron microscopy

Immunogold electron microscopy was performed as previously described (39). Briefly, mice were anesthetized by isoflurane inhalation, and heparin was injected at 100 to 200 U per mouse. Hearts were excised and retrograde perfused with a solution containing 118 mM NaCl, 4.8 mM KCl, 25 mM Hepes, 1.25 mM K_2HPO_4, 1.25 mM $MgSO_4$, and 11 mM glucose (pH 7.4). Mice were perfusion fixed with 4% paraformaldehyde in 0.1 M phosphate buffer (pH 7.4), and hearts were dissected. For immunoelectron microscopy, dissected mice hearts were further fixed in freshly prepared 3% paraformaldehyde in 0.1 M phosphate buffer containing 0.1% glutaraldehyde and 4% sucrose (pH 7.4). Tissues were washed, dehydrated, embedded in Lowicryl K4M (Polysciences, Inc., Warrington, PA), and polymerized under ultraviolet light (360 nm) at −35°C. Ultrathin sections were cut and mounted on Formvar-carbon–coated nickel grids. After incubation with primary antibodies at 4°C overnight, gold-conjugated secondary antibodies [15-nm Protein A Gold, Cell Microscopy Center, University Medical Center Utrecht, 35584 CX Utrecht, The Netherlands; 18-nm Colloidal Gold-AffiniPure Goat Anti-Rabbit IgG (H+L), Jackson ImmunoResearch Laboratories Inc., West Grove, PA] were applied and stained with uranyl acetate and lead citrate by standard methods. Stained grids were examined under Philips CM-12 electron microscope (FEI; Eindhoven, The Netherlands) and photographed with a Gatan (4k × 2.7k) digital camera (Gatan Inc., Pleasanton, CA).

Troponin I measurements

Blood was collected from mice 24 hours post-IR injury. Serum was separated from coagulated blood by centrifugation at 4°C. Serum troponin I levels were measured using the Ultra-Sensitive Mouse Cardiac Troponin-I ELISA (Life Diagnostics, West Chester, PA). The assay was conducted according to the manufacturer's instructions, and measurements were acquired at 450 nm on a Tecan Infinite M1000Pro plate reader.

In vitro IR protocol for isolated adult cardiomyocytes

The suspension of calcium-tolerant adult cardiomyocytes was equally divided into two tubes. One tube was exposed to an ischemia- mimicking buffer as previously described (3, 37, 40). The ischemic buffer was composed of the following: 137 mM NaCl, 3.8 mM KCl, 0.49 mM $MgCl_2$, 0.9 mM $CaCl_2$, and 4.0 mM Hepes supplemented with 10 mM 2-DG, 20 mM sodium lactate, 1 mM sodium dithionite, and 12 mM KCl (pH 6.5). This buffer mimics the is chemic extracellular milieu because it is glucose deficient, hyperkalemic, and acidic/lactate rich. Ischemic cells were additionally placed in a hypoxic chamber (Galaxy 14S, New Brunswick, at 1% O_2), whereas control cells were placed in a regular 5% CO_2 incubator for 45 min. At the end of the ischemic protocol, medium was exchanged to Seahorse medium and reperfusion time initiated. Cells were counted at this step.

Seahorse oxygen consumption measurements

Sodium palmitate (Sigma) was conjugated to fatty acid–free bovine serum albumin (BSA) (Calbiochem) at 1 mM and pH adjusted to 7.4 (41). Seahorse medium was composed of unbuffered DMEM base (Sigma) containing 5 mM glucose, 50 μM palmitate, 200 μM carnitine, and 100 μM pyruvate, pH adjusted to 7.4 at 37°C (41). Adult cardiomyocytes were spun down at 100*g* for 30 s and exposed to Seahorse medium. Cells were then counted and plated at 1500 cells per well on laminin-coated Seahorse 96-well plates. Reperfusion was timed to 1 hour before protocol initiation. Measurements were conducted on the XF96 Seahorse Analyzer. OCR measurements in cardiomyocytes were assured to be stable for the duration of the experiment. Drug-optimized values for maximal responses were as follows: 1.3 μM oligomycin, 1 μM carbonyl cyanide *p*-trifluoromethoxyphenylhydrazone (FCCP), 1 μM rotenone, 1 μM antimycin A, 25 mM 2-DG, and 50 μM etomoxir. At the end of the Seahorse assay, the plate was subjected to a protein assay (Thermo Fisher Scientific) for normalization parameters. Oligomycin was used to inhibit ATP synthase, FCCP was used to deplete the proton gradient, and rotenone/antimycin A was used to inhibit complexes 1 and 3, respectively, thus stopping all mitochondrial-mediated respiration. Glucose oxidation was inhibited by using 2-DG, and fatty acid oxidation was inhibited by using etomoxir. Baseline OCR was determined as the difference between baseline OCR minus nonmitochondrial OCR. ATP-linked OCR was determined as the difference between oligomycin-inhibited respiration (rate 4) and baseline OCR (rate 3). Glucose-mediated respiration was determined as the difference between 2-DG–OCR (rate 4) minus baseline OCR (rate 3). Palmitate-mediated respiration was determined as etomoxir- inhibited respiration (rate 6) minus etomoxir-free respiration (rate 5). For glucose and palmitate OCR graphs, all groups were normalized to WT recordings, which was set to 100%.

PDH activity measurements

Mice were euthanized post-IR injury, and the AAR was quickly removed, frozen, and pulverized. Pulverized tissue was then treated according to manufacturers' protocol (Abcam), with minor modifications. To prevent in vitro posttranslational modifications during sample preparation, apyrase (1×) and phosphatase inhibitor cocktails 2 and 3 (Millipore Sigma) were added to the solubilizing buffer. Apyrase is an enzyme that catabolizes the hydrolysis of ATP and therefore depletes ATP availability for de novo phosphorylation events (42). A PDH enzyme activity microplate assay kit (Abcam) was used to measure enzyme activity. To stay within the linear range of the assay for mouse cardiac tissue, we loaded 60 μg of lysate per well (as shown in the manufacturer's manual). Recordings were acquired on a Tecan Infinite M1000Pro plate reader at 450 nm every minute for 15 min with a 3-s mix between measurements.

^{14}C-glucose oxidation measurements

Glucose oxidation was measured in cardiac tissue from the AAR as previously published (43). Tissue was incubated at 37°C for 1 hour in modified Krebs-Ringer buffer [115 mM NaCl, 2.6 mM KCl, 1.2 mM KH_2PO_4, 10 mM $NaHCO_3$, and 10 mM Hepes (pH7.4)] that contained 2% fatty acid–free BSA, 0.6 mM palmitate, 6 mM glucose, and D-[^{14}C(U)]glucose (5 μCi/ml) and was gassed with 95% O_2 and 5% CO_2. The reaction was terminated, and $^{14}CO_2$ was released by administration of perchloric acid. Released $^{14}CO_2$ was trapped in NaOH-soaked Whatman paper that was placed in the central well of the flasks. A PerkinElmer scintillating counter (model Tri-Carb 2810TR) was used for counting.

Statistical analysis

Experiments were replicated at least three times. Data are means ± SEM. Statistical analysis was performed with Prism (GraphPad) software. Statistical differences between means were analyzed by either an unpaired *t* test or Tukey/Bonferroni post hoc test following two-way ANOVA. Statistical significance was defined as $P < 0.05$.

Supplementary Material

Refer to Web version on PubMed Central for supplementary material.

Acknowledgments:

We thank the team at New York University Langone's Health DART Microscopy Laboratory for EM-related experiments. In addition, we acknowledge inGenious Targeting Laboratories for generating the GRK2-S670A KI mice. **Funding:** The study was supported in part by two Scientist Development Grants from the American Heart Association (to P.Y.S. and to L.A.G.), NIH [grants R37 HL061690, P01 HL075443, and P01 HL091799 to W.J.K.; P01 HL091799 (Core B) to E.G.; and HL130218 to K.D.], and W.W. Smith Charitable Trust (K.D.).

REFERENCES AND NOTES

1. Sato PY, Chuprun JK, Schwartz M, Koch WJ, The evolving impact of G protein-coupled receptor kinases in cardiac health and disease. Physiol. Rev 95, 377–404 (2015). [PubMed: 25834229]
2. Fu X, Koller S, Abd Alla J, Quitterer U, Inhibition of G-protein-coupled receptor kinase 2 (GRK2) triggers the growth-promoting mitogen-activated protein kinase (MAPK) pathway. J. Biol. Chem 288, 7738–7755 (2013). [PubMed: 23362259]

3. Brinks H, Boucher M, Gao E, Chuprun JK, Pesant S, Raake PW, Huang ZM, Wang X, Qiu G, Gumpert A, Harris DM, Eckhart AD, Most P, Koch WJ, Level of G protein-coupled receptor kinase-2 determines myocardial ischemia/reperfusion injury via pro- and anti-apoptotic mechanisms. Circ. Res 107, 1140–1149 (2010). [PubMed: 20814022]
4. Raake PW, Zhang X, Vinge LE, Brinks H, Gao E, Jaleel N, Li Y, Tang M, Most P, Dorn GW II, Houser SR, Katus HA, Chen X, Koch WJ, Cardiac G-protein–coupled receptor kinase 2 ablation induces a novel Ca^{2+} handling phenotype resistant to adverse alterations and remodeling after myocardial infarction. Circulation 125, 2108–2118 (2012). [PubMed: 22496128]
5. Chen M, Sato PY, Chuprun JK, Peroutka RJ, Otis NJ, Ibetti J, Pan S, Sheu S-S, Gao E, Koch WJ, Prodeath signaling of G protein–coupled receptor kinase 2 in cardiac myocytes after ischemic stress occurs via extracellular signal–regulated kinase-dependent heat shock protein 90–mediated mitochondrial targeting. Circ. Res 112, 1121–1134 (2013). [PubMed: 23467820]
6. Obrenovich ME, Smith MA, Siedlak SL, Chen SG, De La Torre JC, Perry G, Aliev G, Overexpression of GRK2 in Alzheimer disease and in a chronic hypoperfusion rat model is an early marker of brain mitochondrial lesions. Neurotox. Res 10, 43–56 (2006). [PubMed: 17000469]
7. Fusco A, Santulli G, Sorriento D, Cipolletta E, Garbi C, Dorn GW II, Trimarco B, Feliciello A, Iaccarino G, Mitochondrial localization unveils a novel role for GRK2 in organelle biogenesis. Cell. Signal 24, 468–475 (2012). [PubMed: 21983013]
8. Lucas E, Jurado-Pueyo M, Fortuño MA, Fernández-Veledo S, Vila-Bedmar R, Jiménez-Borreguero LJ, Lazcano JJ, Gao E, Gómez-Ambrosi J, Frühbeck G, Koch WJ, Díez J, Mayor F Jr., C. Murga, Downregulation of G protein-coupled receptor kinase 2 levels enhances cardiac insulin sensitivity and switches on cardioprotective gene expression patterns. Biochim. Biophys. Acta 1842, 2448–2456 (2014). [PubMed: 25239306]
9. Lucas E, Vila-Bedmar R, Arcones AC, Cruces-Sande M, Cachofeiro V, Mayor F Jr., Murga C, Obesity-induced cardiac lipid accumulation in adult mice is modulated by G protein-coupled receptor kinase 2 levels. Cardiovasc. Diabetol 15, 155 (2016). [PubMed: 27832814]
10. Vila-Bedmar R, Cruces-Sande M, Lucas E, Willemen HLDM, Heijnen CJ, Kavelaars A, Mayor F Jr., Murga C, Reversal of diet-induced obesity and insulin resistance by inducible genetic ablation of GRK2. Sci. Signal 8, ra73 (2015). [PubMed: 26198359]
11. Abd Alla J, Graemer M, Fu X, Quitterer U, Inhibition of G-protein-coupled receptor kinase 2 prevents the dysfunctional cardiac substrate metabolism in fatty acid synthase transgenic mice. J. Biol. Chem 291, 2583–2600 (2016). [PubMed: 26670611]
12. Taguchi K, Hida M, Hasegawa M, Narimatsu H, Matsumoto T, Kobayashi T, Suppression of GRK2 expression reduces endothelial dysfunction by restoring glucose homeostasis. Sci. Rep 7, 8436 (2017). [PubMed: 28814745]
13. Kong G, Penn R, Benovic JL, A β-adrenergic receptor kinase dominant negative mutant attenuates desensitization of the β_2-adrenergic receptor. J. Biol. Chem 269, 13084–13087 (1994). [PubMed: 8175732]
14. Pitcher JA, Tesmer JJG, Freeman JLR, Capel WD, Stone WC, Lefkowitz RJ, Feedback inhibition of G protein-coupled receptor kinase 2 (GRK2) activity by extracellular signal-regulated kinases. J. Biol. Chem 274, 34531–34534 (1999). [PubMed: 10574913]
15. Sato PY, Chuprun JK, Ibetti J, Cannavo A, Drosatos K, Elrod JW, Koch WJ, GRK2 compromises cardiomyocyte mitochondrial function by diminishing fatty acid-mediated oxygen consumption and increasing superoxide levels. J. Mol. Cell. Cardiol 89, 360–364 (2015). [PubMed: 26506135]
16. Polhemus DJ, Gao J, Scarborough AL, Trivedi R, McDonough KH, Goodchild TT, Smart F, Kapusta DR, Lefer DJ, Radiofrequency renal denervation protects the ischemic heart via inhibition of GRK2 and increased nitric oxide signaling. Circ. Res 119, 470–480 (2016). [PubMed: 27296507]
17. Rorabaugh BR, Chakravarti B, Mabe NW, Seeley SL, Bui AD, Yang J, Watts SW, Neubig RR, Fisher RA, Regulator of G protein signaling 6 protects the heart from ischemic injury. J. Pharmacol. Exp. Ther 360, 409–416 (2017). [PubMed: 28035008]
18. Lafarga V, Aymerich I, Tapia O, Mayor F Jr., P. Penela, A novel GRK2/HDAC6 interaction modulates cell spreading and motility. EMBO J 31, 856–869 (2012). [PubMed: 22193721]

19. Gao E, Lei YH, Shang X, Huang ZM, Zuo L, Boucher M, Fan Q, Chuprun JK, Ma XL, Koch WJ, A novel and efficient model of coronary artery ligation and myocardial infarction in the mouse. Circ. Res 107, 1445–1453 (2010). [PubMed: 20966393]
20. Lospachuk GD, Uncoupling proteins as mediators of mitochondrial metabolic rates. Heart Metab 69, 34–37 (2016).
21. Tian R, Understanding the metabolic phenotype of heart disease. Heart Metab. 32, 5–8 (2006).
22. Scheidegger K, Robbins DC, Danforth E Jr., Effects of chronic beta receptor stimulation on glucose metabolism. Diabetes 33, 1144–1149 (1984). [PubMed: 6094291]
23. Patel TB, Olson MS, Regulation of pyruvate dehydrogenase complex in ischemic rat heart. Am. J. Physiol 246, H858–H864 (1984). [PubMed: 6742152]
24. Lopaschuk GD, Metabolic changes in the acutely ischemic heart. Heart Metab. 70, 32–35 (2016).
25. Churchill EN, Murriel CL, Chen C-H, Mochly-Rosen D, Szweda LI, Reperfusion-induced translocation of δPKC to cardiac mitochondria prevents pyruvate dehydrogenase reactivation. Circ. Res 97, 78–85 (2005). [PubMed: 15961716]
26. Elorza A, Penela P, Sarnago S, Mayor F Jr., MAPK-dependent degradation of G protein-coupled receptor kinase 2. J. Biol. Chem 278, 29164–29173 (2003). [PubMed: 12738776]
27. Cassill JA, Whitney M, Joazeiro CA, Becker A, Zuker CS, Isolation of Drosophila genes encoding G protein-coupled receptor kinases. Proc. Natl. Acad. Sci. U.S.A 88, 11067–11070 (1991). [PubMed: 1662381]
28. Ussher JR, Wang W, Gandhi M, Keung W, Samokhvalov V, Oka T, Wagg CS, Jaswal JS, Harris RA, Clanachan AS, Dyck JRB, Lopaschuk GD, Stimulation of glucose oxidation protects against acute myocardial infarction and reperfusion injury. Cardiovasc. Res 94, 359–369 (2012). [PubMed: 22436846]
29. Woo YJ, Taylor MD, Cohen JE, Jayasankar V, Bish LT, Burdick J, Pirolli TJ, Berry MF, Hsu V, Grand T, Ethyl pyruvate preserves cardiac function and attenuates oxidative injury after prolonged myocardial ischemia. J. Thorac. Cardiovasc. Surg 127, 1262–1269 (2004). [PubMed: 15115981]
30. Li T, Zhang Z, Kolwicz SC Jr., Abell L, Roe ND, Kim M, Zhou B, Cao Y, Ritterhoff J, Gu H, Raftery D, Sun H, Tian R, Defective branched-chain amino acid catabolism disrupts glucose metabolism and sensitizes the heart to ischemia-reperfusion injury. Cell Metab. 25, 374–385 (2017). [PubMed: 28178567]
31. Li T, Xu J, Qin X, Hou Z, Guo Y, Liu Z, Wu J, Zheng H, Zhang X, Gao F, Glucose oxidation positively regulates glucose uptake and improves cardiac function recovery after myocardial reperfusion. Am. J. Physiol. Endocrinol. Metab 313, E577–E585 (2017). [PubMed: 28325730]
32. Itoi T, Huang L, Lopaschuk GD, Glucose use in neonatal rabbit hearts reperfused after global ischemia. Am. J. Physiol 265, H427–H433 (1993). [PubMed: 8368344]
33. Merante F, Mickle DA, Weisel RD, Li RK, Tumiati LC, Rao V, Williams WG, Robinson BH, Myocardial aerobic metabolism is impaired in a cell culture model of cyanotic heart disease. Am. J. Physiol 275, H1673–H1681 (1998). [PubMed: 9815075]
34. Huang ZM, Gao E, Fonseca FV, Hayashi H, Shang X, Hoffman NE, Chuprun JK, Tian X, Tilley DG, Madesh M, Lefer DJ, Stamler JS, Koch WJ, Convergence of G protein–coupled receptor and S-nitrosylation signaling determines the outcome to cardiac ischemic injury. Sci. Signal 6, ra95 (2013). [PubMed: 24170934]
35. Fan Q, Chen M, Zuo L, Shang X, Huang MZ, Ciccarelli M, Raake P, Brinks H, Chuprun KJ, Dorn GW II, Koch WJ, Gao E, Myocardial ablation of G protein-coupled receptor kinase 2 (GRK2) decreases ischemia/reperfusion injury through an anti-intrinsic apoptotic pathway. PLOS ONE 8, e66234 (2013). [PubMed: 23805205]
36. Lal H, Ahmad F, Zhou J, Yu JE, Vagnozzi RJ, Guo Y, Yu D, Tsai EJ, Woodgett J, Gao E, Force T, Cardiac fibroblast glycogen synthase kinase-3β regulates ventricular remodeling and dysfunction in ischemic heart. Circulation 130, 419–430 (2014). [PubMed: 24899689]
37. Woodall MC, Woodall BP, Gao E, Yuan A, Koch WJ, Cardiac fibroblast GRK2 deletion enhances contractility and remodeling following ischemia/reperfusion injury. Circ. Res 119, 1116–1127 (2016). [PubMed: 27601479]

38. Grisanti LA, Traynham CJ, Repas AA, Gao E, Koch WJ, Tilley DG, β2-Adrenergic receptor-dependent chemokine receptor 2 expression regulates leukocyte recruitment to the heart following acute injury. Proc. Natl. Acad. Sci. U.S.A 113, 15126–15131 (2016). [PubMed: 27956622]

39. Kerr DE, Liang F, Bondioli KR, Zhao H, Kreibich G, Wall RJ, Sun T-T, The bladder as a bioreactor: Urothelium production and secretion of growth hormone into urine. Nat. Biotechnol 16, 75–79 (1998). [PubMed: 9447598]

40. Punn A, Mockridge JW, Farooqui S, Marber MS, Heads RJ, Sustained activation of p42/p44 mitogen-activated protein kinase during recovery from simulated ischaemia mediates adaptive cytoprotection in cardiomyocytes. Biochem. J 350 (Pt. 3), 891–899 (2000). [PubMed: 10970806]

41. Readnower RD, Brainard RE, Hill BG, Jones SP, Standardized bioenergetic profiling of adult mouse cardiomyocytes. Physiol. Genomics 44, 1208–1213 (2012). [PubMed: 23092951]

42. Tran JH, Chen C-J, Emr S, Schekman R, Cargo sorting into multivesicular bodies in vitro. Proc. Natl. Acad. Sci. U.S.A 106, 17395–17400 (2009). [PubMed: 19805166]

43. Drosatos K, Pollak NM, Pol CJ, Ntziachristos P, Willecke F, Valenti M-C, Trent CM, Hu Y, Guo S, Aifantis I, Goldberg IJ, Cardiac myocyte KLF5 regulates *Ppara* expression and cardiac function. Circ. Res 118, 241–253 (2016). [PubMed: 26574507]

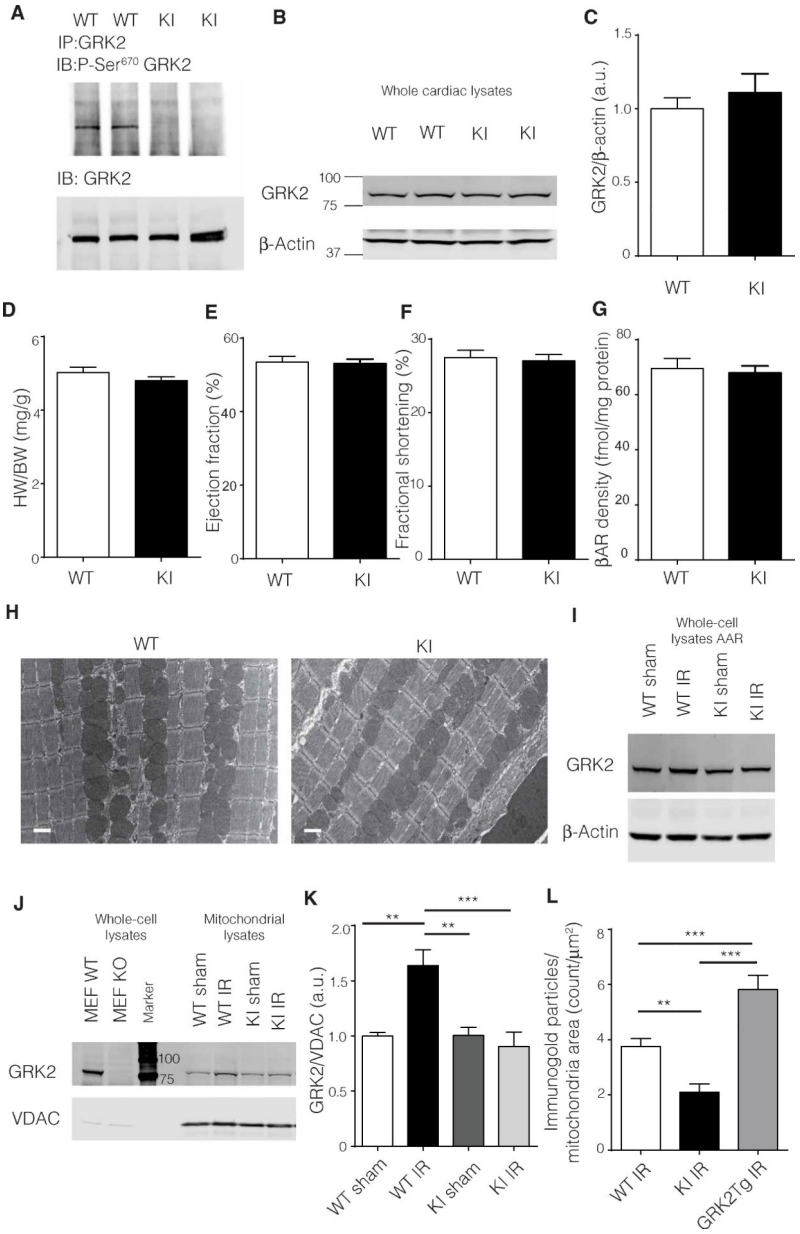

Fig. 1. A normal cardiac phenotype in GRK2-S670A KI mice and mitochondrial translocation of GRK2 post-IR injury.

(A) GRK2 immunoprecipitates (IP) from WT or KI cardiac lysates were immunoblotted (IB) for total GRK2 or phospho (P)–Ser^{670} (n = 6 hearts per genotype). (**B**) Whole cardiac lysates from WT and KI animals were immunoblotted for total GRK2 and β-actin as a loading control. (**C**) Quantification of (B) (n = 8 hearts per genotype). (**D**) Heart weight–to–body weight (HW/BW) parameters in KI and WT mice (n = 13 to 20 hearts per genotype). (**E**) In vivo cardiac function as assessed by ejection fraction percentage determined by echocardiography (n = 25 to 26 hearts per genotype). (**F**) Left ventricular (LV) fractional shortening percentage determined by echocardiography (n = 25 to 26 hearts per genotype). (**G**) Radioligand binding results of myocardial sarcolemmal βAR levels in WT and KI cardiac lysates (n = 7 hearts per genotype). (**H**) Representative transmission electron

microscopic images of cardiac tissue from WT and KI (n = 3 hearts per genotype). Scale bars, 1 μm. (**I**) Whole-cell lysates from the AAR in WT and KI hearts post-IR injury (24 hours) were immunoblotted for total GRK2 levels (n = 4 to 6 hearts per group). Quantification is shown in fig. S3A. (**J**) Purified mitochondrial fractions from the AAR in WT and KI hearts were immunoblotted for GRK2. Whole-cell lysates from mouse embryonic fibroblasts derived from WT and GRK2 knockout mice were used as positive and negative control for the blots. (**K**) Quantification of protein immunoblots shown in (J) (n = 5 to 8 hearts per group). (**L**) Sections from the AAR in WT and KI hearts post-IR injury were immunogold labeled for GRK2. GRK2 immunogold labeling of sections from transgenic mice overexpressing GRK2 was used as control. Representative images are shown in fig. S3B (n = 20 to 24 images from three hearts per genotype). Statistical significance was determined by Student's t test or analysis of variance (ANOVA). Data are shown as means ± SEM; *P < 0.05, **P < 0.01, ***P < 0.005. a.u., arbitrary units.

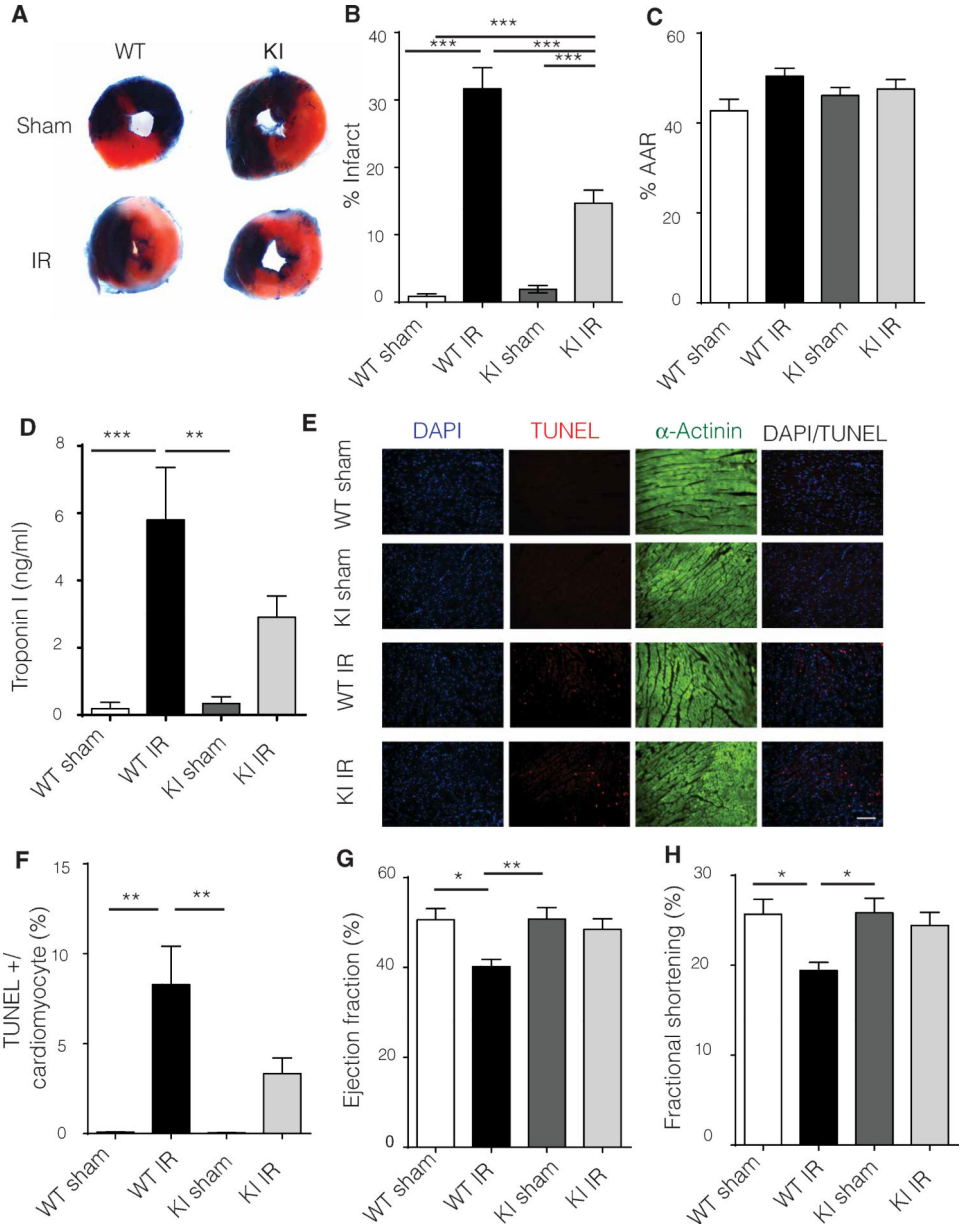

Fig. 2. Limiting mitochondrial GRK2 translocation post-IR injury significantly reduces LV infarct size through diminished myocyte cell death.

(**A**) Representative Evans blue staining of hearts 24 hours after IR injury of WT and KI mice. Blue area is the area not at risk (ANAR), red is the AAR, and white represents the infarct. (**B**) Quantification of Evans blue staining (n = 19 to 20 hearts per group). (**C**) %AAR or the area subjected to injury in WT and KI mice (n = 19 to 20 hearts per group). (**D**) Serum troponin I levels were measured 24 hours post-IR injury in WT and KI mice (n = 5 to 6 mice per group). (**E**) TUNEL (red) analysis of cardiac tissue from WT and KI mice counterstained with β-actinin (green) to visualize cardiomyocytes; 4′,6-diamidino-2-phenylindole (DAPI) was used as a nuclear marker (blue). Scale bar, 100 μm. (**F**) TUNEL quantification of images in (E) (n = 3 to 5 hearts per group). (**G**) Echocardiography ejection fraction percentage in WT and KI mice 24 hours post-IR injury reveals improved cardiac

function in the KI animals (n = 19 to 20 mice per group). (**H**) LV fractional shortening percentage as determined by echocardiography (n = 19 to 20 mice per group). Statistical significance was determined by ANOVA. Data are shown as means ± SEM; *P < 0.05, **P < 0.01, ***P < 0.005.

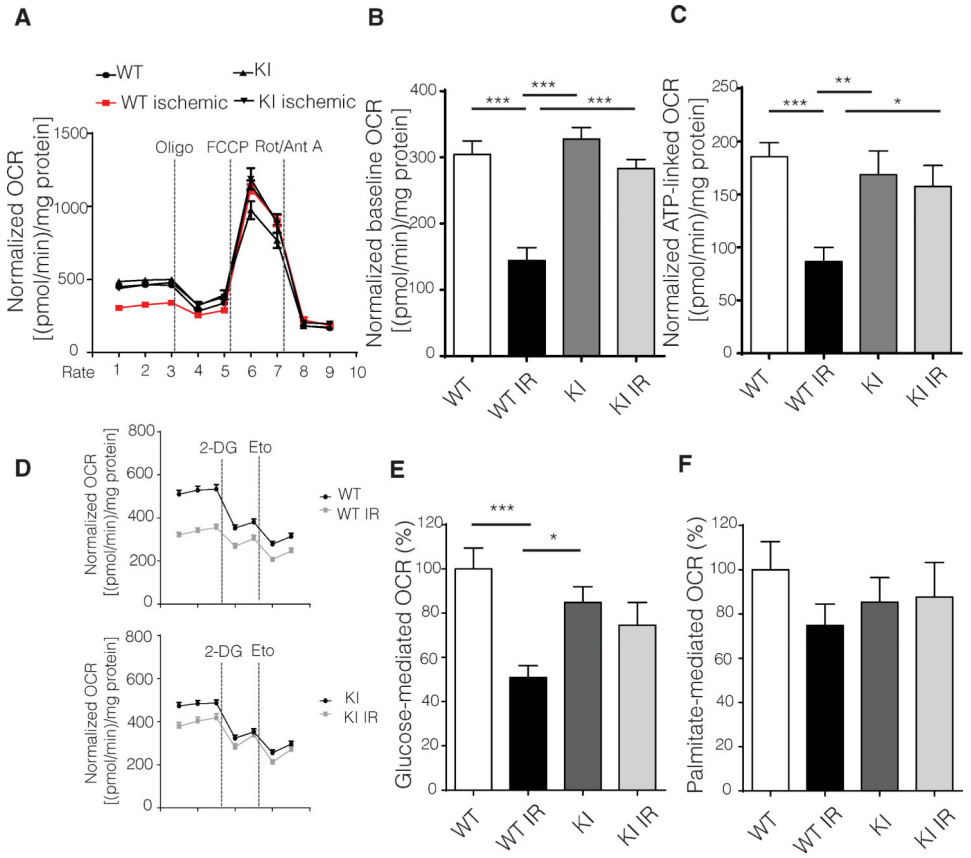

Fig. 3. Adult cardiomyocytes from GRK2-S670A KI mice post-IR injury maintain mitochondrial respiration and a normal glucose respiratory response.

(**A**) OCRs measured using a Seahorse flux analyzer in cardiomyocytes isolated from post-IR injury (24 hours) WT and KI mice (n = 44 to 47 wells per group; data from three hearts per genotype and all data normalized to total protein content). Oligo, oligomycin; Rot, rotenone; Ant A, antimycin A. (**B**) Quantification of basal respiration from data in (A); n same as in (A). (**C**) Quantification of ATP production from data in (A); n same as in (A). (**D**) Seahorse tracings of OCRs in cardiomyocytes from WT and KI mice post-IR injury normalized to protein content (n = 27 to 36 wells from three hearts per genotype). Eto, etomoxir. (**E**) Quantification of glucose- mediated respiration shown in (D); n values same as in (D). (**F**) Quantification of palmitate-mediated respiration shown in (D); n values same as in (D), ANOVA. Data are shown as means ± SEM; *P < 0.05, **P < 0.01, ***P < 0.005.

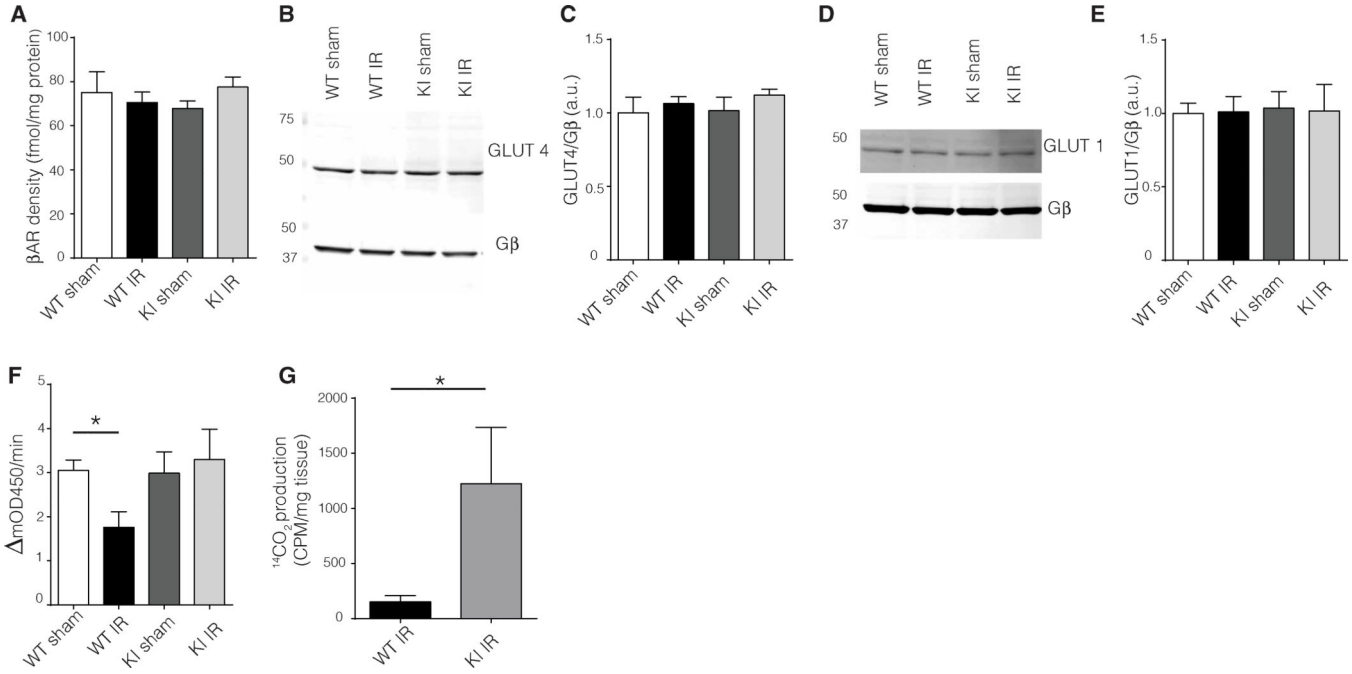

Fig. 4. Defective mitochondrial GRK2 translocation post-IR injury improves glucose respiration by modulating PDH activity and glucose oxidation.

(**A**) Radioligand binding studies of βAR in cardiac sarcolemmal membranes from WT or KI mice post-IR injury (n = 4 hearts per group). (**B** and **C**) Representative Western blots for plasma membrane GLUT4 in the AAR (B) and quantification (C). Gβ was used as loading control for the plasma membrane preparations (n = 4 hearts per group). (**D** and **E**) Representative Western blot for plasma membrane GLUT1 in the AAR (D) and quantification (E). Gβ was used as loading control for the plasma membrane preparations (n = 4 hearts per group). (**F**) PDH activity assay in pulverized cardiac tissue from the AAR (n = 7 to 9 hearts per group). (**G**) Radioactive glucose oxidation measurements from AAR samples (n = 6 to 7 hearts per genotype). CPM, counts per minute. ANOVA and Student's t test. Data are shown as means ± SEM; *P < 0.05.